Pergamon

PII:S0022-3697(96)00230-2

J. Phys. Chem Solids Vol 58, No. 7, pp. 1161–1165, 1997

0022-3697/97 $17.00 + 0.00

PHASE TRANSITION INDUCED CURRENT CARRIER INJECTION PHENOMENON IN GRAPHITE INTERCALATION COMPOUNDS

A. M. ZIATDINOV and N. M. MISHCHENKO

Institute of Chemistry, Russian Academy of Sciences, 100-let Vladivostoku, 159, 690022 Vladivostok, Russia

(*Received* 28 *May* 1995; *accepted* 31 *May* 1995)

Abstract—In graphite intercalation compounds $C_{20}HNO_3$ we have observed a similar dependence of conductivity, conduction electron spin resonance (CESR) linewidth and spin carrier concentration versus temperature. It was shown that the increase of conductivity and 'nonmetallic' broadening of the CESR linewidth observed at and after crystallization of the HNO_3 'guest' molecules may be due to an increase in concentration of conduction electrons and a decrease in their mobility, respectively. © 1997 Elsevier Science Ltd. All rights reserved.

Keywords: A. metals, B. chemical synthesis, D. order–disorder effects, E. electron paramagnetic resonance.

INTRODUCTION

The temperature dependence of the conduction electron spin resonance (CESR) linewidth (ΔH) in metals is successfully explained [1] in terms of Elliot's theory [2], according to which $\Delta H = \alpha(\Delta g)^2/\tau$, where α is a constant, Δg is the g-shift from the free electron value, and τ is the conductivity relaxation time. Upon cooling of metals the frequency of the electron–electron and electron–phonon collisions decreases and, as a result, τ increases, while the concentration of the current carriers (N) remains practically constant because of high values of Fermi temperature [3]. As a result, as the temperature is lowered, the conductivity of pure metals $\sigma = Ne^2\tau/m^* = Ne\mu$ (where m^*, e and μ are the effective mass, charge and mobility of charge carriers, respectively) increases and, simultaneously, the CESR linewidth decreases. In this paper we report a new physical situation found in acceptor graphite intercalation compounds (GICs) $C_{20}HNO_3$, when both the basal plane and the c-axis components of the electroconductivity and the CESR linewidth dependences versus temperature are similar, and we present the results of an investigation of this phenomenon.

EXPERIMENTAL

GICs comprise a wide class of synthetic metals and present an alternating sequence of n hexagonal graphite monolayers (where n is the stage index) and a monolayer of 'guest' atoms or molecules (the intercalate) [4]. The $C_{20}HNO_3$ compounds investigated belong to the fourth stage of α-modification of GICs with nitric acid, with the general formula $C_{5n}HNO_3$ ($n = 1, 2, 3 \ldots$) [4, 5]. According to data from various physical methods [4], in these GICs the two-dimensional liquid-like layers of HNO_3 are ordered and form a two dimensional crystal at temperatures lower than $T_c \sim 250$ K. Layers of HNO_3 may be incommensurable with a carbon net along one of its crystallographic directions and they undergo a structural phase transition of the incommensurate phase–commensurate phase type at $T \sim 210$ K [6].

CESR spectra of GIC $C_{20}HNO_3$ plates were registered at the X-band ($\nu = 9.52$ GHz) in the temperature range of 90–300 K using a rectangular resonator with the TE_{102} mode and 2.5 kHz modulation of an external constant magnetic field H_o. At the conventional setting of the rectangular resonator, the electric component of the microwave field is parallel to H_o; in the geometric center of the resonator the magnetic component of the microwave field (H_{rf}) is parallel to the vertical axis of the resonator.

Highly oriented pyrolitic graphite plates required for GIC synthesis were cut out of a single bar with the basal plane conductivity equal to $(1.3 \pm 0.2) \times 10^4\ \Omega^{-1}\,cm^{-1}$. These plates had the shape of a rectangular parallelepiped with dimensions of l (width) $\times$ h (height) $\times$ d (thickness), where $l \times h$ is the square of the basal plane. The accuracy in determining the size of the plates was $\sim 5 \times 10^{-4}$ cm. Synthesis of GIC $C_{20}HNO_3$ was carried out in nitric acid with a density $\rho = 1.47\ g\,cm^{-3}$. The GIC stage was controlled by the diffraction method. The effect of temperature on CESR lineshape parameters was investigated using a plate with dimensions of $0.40 \times 0.40 \times 0.02\ cm^3$.

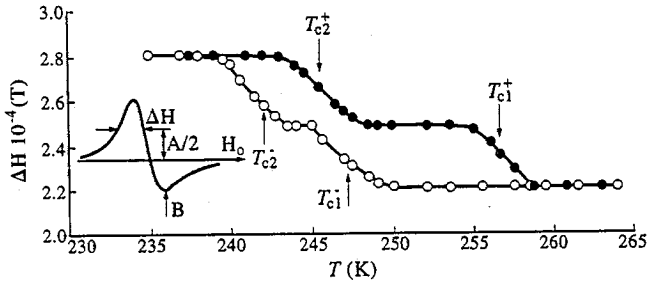

Fig. 1. Temperature dependence of CESR linewidth ΔH of $C_{20}HNO_3$ plate with dimensions $0.4 \times 0.4 \times 0.02\,cm^3$ at crystallization and melting of intercalate. Unfilled (filled) symbols correspond to experimental values of parameters on cooling (heating) of the GIC. T_{c1}^- (T_{c1}^+) and T_{c2}^- (T_{c2}^+) are the temperatures of the first and second stepwise increase (decrease) of ΔH on cooling (heating) of the sample, respectively. $H_o \perp c$; $\nu = 9.52$ GHz.

RESULTS AND DISCUSSION

Over the entire temperature range of the investigations a single asymmetric CESR signal of $C_{20}HNO_3$ is observed. Down to ~250 K the asymmetry parameter of the first derivative of the absorption line A/B (which is defined as the ratio of the maximum peak height (A) to the minimum peak height (B), both measured with respect to the zero-line of the resonance derivative) and the width (ΔH) of the CESR line at half the height of the peak A are independent of temperature and are equal to 3.2 ± 0.1 and 2.20×10^{-4} T, respectively. At all temperatures the spectrum is axial with respect to the c-axis and is characterized by $g_\parallel = 2.0023 \pm 0.0001$ and $g_\perp = 2.0028 \pm 0.0001$. At $T_{c1}^- \sim 247$ K, $T_{c2}^- \sim 242$ K and $T_{c3} \sim 212$ K the ΔH undergoes a stepwise increase and continues to increase as the temperature decreases (Figs 1 and 2). As the temperature increases, the ΔH values change inversely, but with a 'global' temperature hysteresis (Figs 1 and 2). The value of A/B slightly decreases at temperatures lower than T_{c1}^- and is equal to 2.8 ± 0.1 at 90 K. The temperatures of the stepwise changes in ΔH, $T_{c1}^{\pm}$ and $T_{c2}^{\pm}$, are close to the temperature of intercalate crystallization (melting) in $C_{20}HNO_3$ ($T_c \sim 250$ K) known from the literature [4]. This allows us to treat the CESR lineshape transformations observed in $C_{20}HNO_3$ at $T_{c1}^{\pm}$ and $T_{c2}^{\pm}$ as being due to the change in the aggregate state of the 'guest' molecules. The CESR lineshape transformation at T_{c3} is probably due to the incommensurate phase–commensurate phase type transition. At microwave field power levels far from saturation and the same temperature, ΔH values in the Q- and X-bands coincide, indicating that the CESR line is homogeneously broadened.

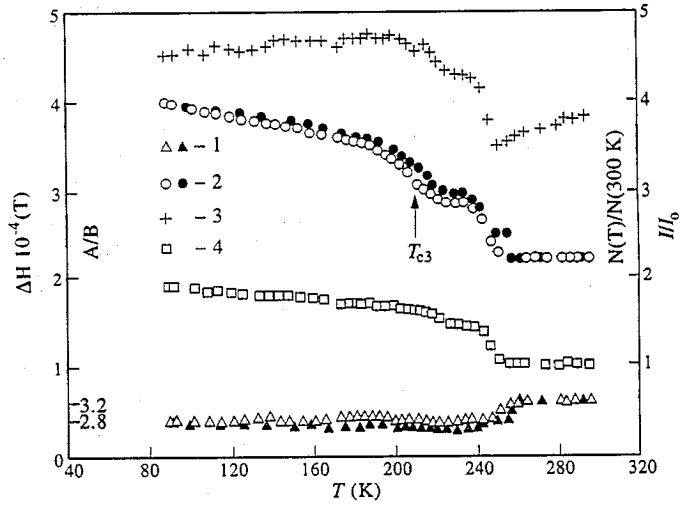

Fig. 2. Dependence of parameters of the CESR line of $C_{20}HNO_3$ plate with dimensions $0.4 \times 0.4 \times 0.2\,cm^3$, i.e. A/B (curve 1), ΔH (curve 2) and I/I_o (curve 3), where I_o is the intensity of the Mn^{2+} ESR line in a standard sample ($ZnS:Mn^{2+}$), on temperature at crystallization and melting of the intercalate. Curve 4 corresponds to the dependence: $N(T)/N(300\,K) = [I(T)/I(300\,K)][\sigma_c(T)/\sigma_c(300\,K)]^{1/2}$, where $I(T)$ is an experimental value of the intensity and the value of $\sigma_c(T)$ is determined by the linear functions $[(-6.52 \times 10^{-3}/K)T + 3.56](\Omega\,cm)^{-1}$ and $[(-8.46 \times 10^{-3}/K)T + 4.6](\Omega\,cm)^{-1}$ for $T > T_{c1}^-$ and $T < T_{c1}^-$, respectively. Unfilled (filled) symbols correspond to experimental values of parameters on cooling (heating) of the GIC. T_{c3} is the temperature of the third stepwise change of ΔH. $H_o \perp c$; $\nu = 9.52$ GHz.

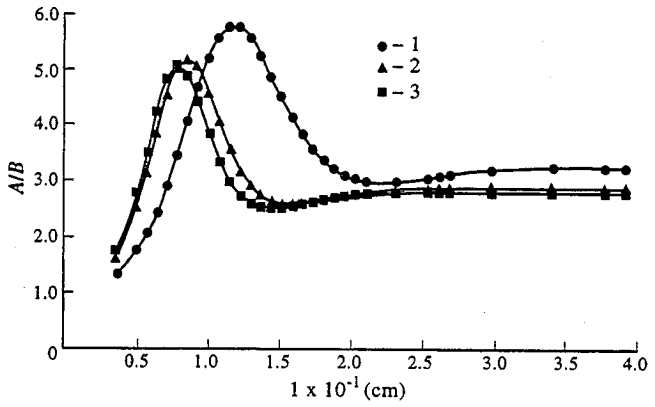

Fig. 3. Experimental (filled symbols) and theoretical (solid lines) values of the line asymmetry ratio A/B of $C_{20}HNO_3$ plates with dimensions $1 \times 0.4 \times 0.02\,cm^3$ on sample width (l). Experimental curves 1, 2 and 3 correspond to 300, 220 and 174 K, respectively. $H_o \perp c$; $\nu = 9.52$ GHz. The theoretical curves at 300, 220 and 174 K are one-dimensional Dyson's curves with $\sigma_c = 1.6$, 2.74 and 3.13 $(\Omega\,cm)^{-1}$, $R_a = 1.2$, 1.8 and 2.1, and $T_2 = \hbar(g_\perp \beta \Delta H)^{-1} = 2.84 \times 10^{-8}$, 2.1×10^{-8} and 1.97×10^{-8} s, respectively (where β is the Bohr magneton).

The basal plane electroconductivity (σ_a) of $C_{20}HNO_3$ plates was measured by a contactless induction method using a device analogous to that described by Pendrys *et al.* [7]. Saint-Jean and McRae [8] recommended the contactless method to determine the c-axis electroconductivity (σ_c), using the well known A/B vs $1/\delta_c$ nomograms and narrow samples with $1/\delta_c < 2.5$ (where δ_c is the skin-depth determined by the σ_c conductivity). At $1/\delta_c < 2.5$, the ratio of A/B does not depend on spin carrier mobility [8]. This enables one to determine the value of δ_c and, consequently, the value of σ_c unambiguously, by measuring the values of A/B and l. However, in narrow samples of GICs with HNO_3 [9], as well as in narrow samples of GICs with AsF_5 [8], the values of σ_c and the two-dimensional diffusion constant depend on the sample width. This unusual result for narrow GIC samples is probably connected with the fact that the intercalate layer composition depends on sample dimensions [8]. That is why, in this study, another contactless method was used to determine the value of σ_c. Here it was determined by locating the coordinate of the maximum l_{max} of the $A/B(l)$ dependence. At a given frequency of the microwave field the values of l_{max} and σ_c are unambiguously related [10]. In this case the $A/B(l)$ dependence was preliminarily studied in more detail at a fixed temperature both before and after the phase transition (Fig. 3). It was established that, as the temperature decreases, both electroconductivity components increase (Fig. 4). Thus, in $C_{20}HNO_3$, at and after crystallization of the intercalate, the electroconductivity and ΔH increase. This observation contradicts the existing considerations on the character of the relation between these quantities in pure metals. We have found the explanation for this contradiction by investigating the effect of temperature on N and the mobility of the spins along the carbon layers μ_a.

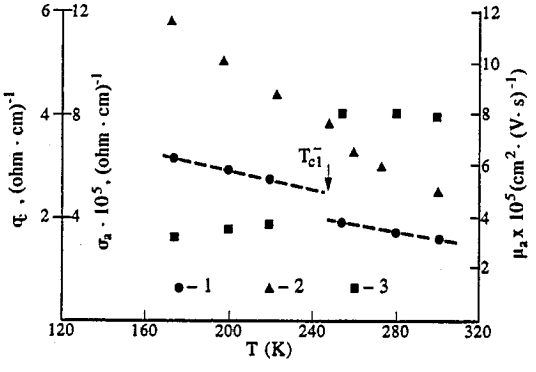

Fig. 4. Temperature dependence of σ_c (1), σ_a (2) and μ_a (3) in $C_{20}HNO_3$. The dashed line corresponds to the linear function $\sigma_c = [(-6.52 \times 10^{-3}/K)T + 3.56](\Omega\,cm)^{-1}$ and $\sigma_o = [(-8.46 \times 10^{-3}/K)T + 4.6](\Omega\,cm)^{-1}$ for $T > T_{cl}^-$ and $T < T_{cl}^-$, respectively.

In the microwave field of a given configuration only the conduction plate regions adjacent to the vertical faces (*hxl*) and (*hxd*) and situated approximately within the skin-depth contribute to the CESR [10, 11]. In $C_{20}HNO_3$, due to the high conduction anisotropy ($\sim 10^5$) one may neglect the contribution to CESR from regions adjacent to the basal planes (*hxl*). This peculiarity of $C_{20}NHO_3$ plates allows us to analyze their CESR lineshape using the one-dimensional Dyson expressions [12] for CESR lineshape in isotropic metals and Feher and Kip [13] or Kodera [14] nomograms calculated from the Dyson expressions [12]. In particular, using the values of A/B and ΔH and Feher and Kip [13] nomograms one can easily determine the value T_{Da}—the spin diffusion time along basal planes across the skin-depth δ_c. According to Dyson [12], in the approximation of independent

electrons the value T_{D_a} is connected with the inplane spin diffusion coefficient D_a by the relation $D_a = \delta_c^2/2 \cdot T_{D_a}$. In its turn, the value μ_a is connected with the value D_a via the Einstein relation for diffusion processes, $\mu_a = eD_a/kT$. The estimation of μ_a according to these expressions has shown (Fig. 4) that its value at and after intercalate crystallization decreases.

If in the GICs investigated the spin carrier mobility is proportional to the current carrier mobility, then the simultaneous increase in σ_a and decrease in μ_a which takes place in $C_{20}HNO_3$ at and after intercalate crystallization, already indicates an increase of N, since $\sigma_a = Ne\mu_a$. Analysis of the temperature dependence of the CESR signal integral intensity $I = (A + B)\Delta H^2$ (Fig. 2) supports this conclusion. In fact, for a given geometry of the sample $I \sim N\delta_c$. Because of this, the simultaneous increase in I and decrease in δ_c which takes place in $C_{20}HNO_3$ as the temperature decreases from T_{c1}^- to T_{c3}, suggests that N increases over this temperature range. This conclusion does not change once the 6.7% increase in I (relative to its value in the liquid phase of the intercalate) according to the decrease in A/B in this temperature range has been taken into consideration by a standard procedure [13, 14]. Using this relation and approximating the experimental values of σ_c before and after phase transition by the linear functions $[(-6.52 \times 10^{-3}/K)T + 3.56](\Omega\,\mathrm{cm})^{-1}$ and $[(-8.46 \times 10^{-3}/K)T + 4.6](\Omega\,\mathrm{cm})^{-1}$, respectively, we have calculated the dependence (Fig. 2):

$$N(T)/N(300\,\mathrm{K}) = [I(T)/I(300\,\mathrm{K})][\sigma_c(T)/\sigma_c(300\,\mathrm{K})]^{1/2}.$$

As would be expected from the results of the qualitative analysis of the experimental data, in the crystal phase of the intercalate N increases as the temperature is lowered (Fig. 2). Concerning the behaviour of N in the quasiliquid phase of the intercalate, all its variations occur within the limits of experimental error (Fig. 2). By summing the results of the experimental data analysis, one can conclude that in synthetic metal $C_{20}HNO_3$ in the solid phase of the intercalate (over the entire temperature range of the investigations) the increase in σ_a is at least partially due to an increase in N, whereas the broadening of the CESR line at and after crystallization of the intercalate is essentially due to the decrease in τ_a.

The broadening of the CESR line is homogeneous. The g-tensor values of spin carriers are independent on the changes in aggregate states of the intercalate and they are close to the g-tensor value of a free electron. These facts testify that the density of the probability of charge carriers on intercalate molecules is small and does not change at phase transition. The foregoing shows that it is possible to analyze the transformations of the electronic properties of $C_{20}HNO_3$ induced by phase transition in terms of the rigid electronic band model of GICs [4, 15]. In terms of this model, in acceptor GICs related to conductors with the hole Fermi surface [4], an increase in N as the temperature decreases is possible only with a lowering of the Fermi energy, for instance due to the transfer of additional electrons from carbon layers to intercalate layers [4, 15], or due to the localization of spin carriers in graphite layers, preferentially at the edges of the Dumas–Herold islands [16]. In this case, an increase in N must obviously be accompanied by a decrease in μ_a and an increase in ΔH, because the localized electrons are the perturbation centers for the conduction electrons. That is, in the crystal phase of the 'guest' molecule subsystem, the rigid electronic band model predicts, qualitatively, the correct temperature effect for these experimental values. Note that several recent experimental results confirm the existence in GICs of localized moments and traps. For instance, Davidov *et al.* [17] observed, using spin-echo techniques performed on AsF_5 GICs, the presence of localized magnetic moments in the graphite layers and suggested the existence of traps. A precise analysis of the spin-relaxation time [8] and the anisotropy of the linewidth with respect to the orientation of H_0 [18] confirms this assumption. At the present time, the exact nature of these traps remains to be determined.

Acknowledgements—The authors are grateful to L. B. Nepomnyashchii (State Research Institute of Graphite, Moscow) for the HOPG plates used in the synthesis of GIC. This work was supported by a grant from the Russian Foundation of Basic Research (N 97-03-33346a).

REFERENCES

1. Monod, P. and Beuneu, F., *Phys. Rev. B*, 1979, **19**, 911.
2. Elliot, R. J., *Phys. Rev.*, 1954, **96**, 266.
3. Madelung, O., *Festkorpertheorie*, Vols I and II. Springer-Verlag, Berlin, 1972.
4. Dresselhaus, M. S. and Dresselhaus, G., *Adv. Phys.*, 1981, **30**, 139.
5. Bottomly, M. J., Parry, G. S. and Ubbelohde, A. R., *Proc. Roy. Soc. London*, 1964, **A279**, 291.
6. Batallan, F., Rosenman, I., Magerl, A. and Fuzellier, H., *Phys. Rev. B*, 1985, **32**, 4810.
7. Pendrys, L. A., Zeller, C. and Vogel, F. L., *J. Mat. Sci.*, 1980, **15**, 2103.
8. Saint-Jean, M. and McRae, E., *Phys. Rev.*, 1991, **43**(5), 3969–3974.
9. Ziatdinov, A. M. and Mishchenko, N. M., Extended Abstracts of the 27th Congress AMPERE, 1994, Vol. 1, 543.
10. Ziatdinov, A. M. and Mishchenko, N. M., *Fizika Tverdogo Tela (Russia)*, 1994, **36**, 8360.

11. Blinowski, J., Kacman, P., Rigaux, C. and Saint-Jean, M., *Synth. Met.*, 1985, **12**, 419.
12. Dyson, F. J., *Phys. Rev.*, 1955, **98**, 349.
13. Feher, G. and Kip, A. F., *Phys. Rev.*, 1955, **98**, 337.
14. Kodera, H., *J. Phys. Soc. Jpn*, 1970, **28**, 89.
15. Leung, S. Y. and Dresselhaus, G., *Phys. Rev. B*, 1981, **24**, 3490.
16. Ziatdinov, A. M., Mishchenko, N. M. and Nikolenko, Yu. M., *Synth. Met.*, 1993, **59**, 253.
17. Davidov, D., Grupp, A., Kass, H. and Hoffer, P., *Synth. Met.*, 1988, **23**, 291.
18. Shimamura, S., *Synth. Met.*, 1985, **12**, 365.